Anomalous Schottky Barriers and Contact Band-to-Band Tunneling in Carbon Nanotube Transistors

David J. Perello,[†] Seong ChuLim,[‡] Seung Jin Chae,[‡] Innam Lee,[†] Moon. J. Kim,[§] Young Hee Lee,[‡,*] and Minhee Yun[†,*]

[†]Department of Electrical Engineering, University of Pittsburgh, Pittsburgh, Pennsylvania 15219, [‡]Department of Physics, Department of Energy Science, Sungkyunkwan Advanced Institute of Nanotechnology, Suwon 440-746, Republic of Korea, and [§]Department of Materials Science and Engineering, University of Texas—Dallas, Richardson, Texas 75080

ABSTRACT Devices incorporating nanoscale materials, particularly carbon nanotubes (CNTs), offer exceptional electrical performance. Absent, however, is an experimentally backed model explaining contact-metal work function, device layout, and environment effects. To fill the void, this report introduces a surface-inversion channel model based on low temperature and electrical measurements of a distinct single-walled semiconducting CNT contacted by Hf, Cr, Ti, and Pd electrodes. Anomalous barrier heights and metal-contact dependent band-to-band tunneling phenomena are utilized to show that, dependent upon contact work function and gate field, transport occurs either directly between the metal and CNT channel or indirectly *via* injection of carriers from the metal-covered CNT region to the CNT channel. The model is consistent with previously contradictory experimental results, and the methodology is simple enough to apply in other contact-dominant systems.

KEYWORDS: carbon nanotubes · Schottky barrier · electrical transport · band to band tunneling · work function

Carbon nanotube field effect transistors (CNT-FETs) have high current-carrying capability,[1] on/off ratio greater than 10^6,[2−4] and switchable polarity dependent upon environment and chemical treatment.[5,6] Rapid optimization and performance enhancement in CNT-FETs has occurred.[7] Nevertheless, the physics and the underlying mechanisms for transport are still incomplete. For instance, experimentally distinguishing energy band alignment at the metal−CNT contact has proven to be exceedingly difficult[8,9] and scarce experimental evidence exists in the form of Schottky barrier heights. Initially, it was believed that gas adsorbates in the CNT channel induce a charge transfer from CNTs to adsorbates, resulting in p-type conduction in ambient measurement conditions.[10,11] However, more recently it was argued that the adsorbate-induced planar dipole layers at the interface are the key factor for determining the majority carrier.[12]

The model of the induced dipole layer at the interface generally explains the CNT device operation. For Au contacts, conduction variations are attributed to the induced dipole moment due to oxygen adsorbates at the interface. In the absence of oxygen, Au electrons are spilled over to CNT. In the presence of oxygen however, strong charge transfer occurs from Au to oxygen, forming a dipole opposed to the spillover.[13] This dipole layer depletes the CNT, pulling the Fermi level (E_F) of CNT toward the valence band maximum. Similarly, in the case of Ti, a commonly used contact metal, oxygen-induced surface potential variations were introduced to explain the dominant p-type behavior.[12] However, contrary to these earlier reports, McClain *et al.* observed that under atmospheric O_2 exposure, the range of off-state gate bias was extended significantly into the n-region until the electron conducting on-state weakly appeared.[14] This occurrence cannot be explained by a planar dipole model, nor is it consistent with an earlier oxygen doping model. The formation of a dipole layer at the interface (due to oxygen in this case) should give rise to a threshold voltage change exclusively. Conversely, increases in dopant (oxygen) concentrations should be followed by a significant increase in off-current[15] in contrast to the CNT devices which often exhibit the reverse phenomenon.

In a circuit with multiple current paths, carriers will always traverse the path with the lowest resistance, even if the physical length of such a path is longer. When contacted with low work function metals, the electron contribution of the subsurface metal-covered CNT is often neglected because of the longer conduction pathway

*Address correspondence to leeyoung@skku.edu, miy16@pitt.edu.

Received for review February 17, 2010 and accepted May 19, 2010.

Published online May 28, 2010. 10.1021/nn100328a

© 2010 American Chemical Society

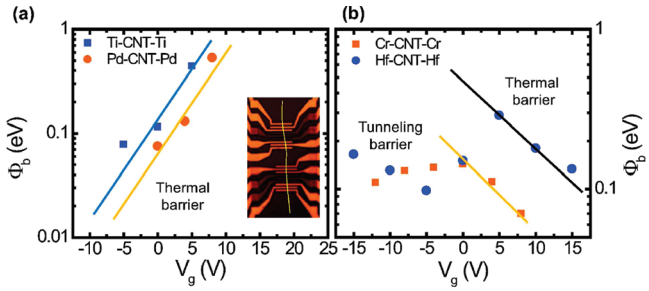

Figure 1. (a) Schottky barriers extracted by using the thermionic model and activation energy measurements: Ti (square) and Pd (circle) barrier heights as a function of gate voltage. Inset is an optical image of the device layout used for measurements. The solid line denotes the location of the single CNT used for all the measurements with four different metal electrodes. (b) Schottky barrier heights for low-work-function metals Cr (square) and Hf (circle). The solid lines indicate least-squares fit of the data in the range.

compared to that of the metal edge-to-CNT path. As a result, the interface-dominant conduction of the surface dipole model is inconsistent with conduction in extremely low work function metals where surface-passivated metal contacts with work functions $\ll$4.0 eV have usually been required for stable electron conduction.[4,16] These inconsistencies (as well as our observations in this report) suggest that an updated model is required to accommodate such complications in the transport phenomena at the metal−CNT contact.

Knowledge of the aforementioned lack of measured Schottky barrier magnitudes is crucial to development of said model. For example, the magnitude of the Schottky barrier over a range of applied gate bias (V_g) will provide the energy band offsets and alignments, while the slope of the barrier *versus* gate bias will provide information with respect to the nature of the dominant carrier (electron, hole, or both). These measurements must be performed for devices located on a single, distinct, CNT, since contact Schottky barriers on different CNTs and results from different groups may also induce further complications as a result of the variable diameter CNTs and fabrication conditions adopted. For consistent data acquisition and clear understanding of results, different metal contacts must all be fabricated on one single-walled CNT, using identical fabrication conditions and testing environments.

The purpose of this report is 2-fold: (i) to fabricate numerous CNT devices on one long single-walled CNT with multiple metals as contacts and (ii) to construct a new model for transport not only to explain our measurements but also to resolve discrepancies in the previous models. To accomplish this, various metal contacts (Hf, Cr, Ti, and Pd) were fabricated on a single chemical vapor deposition grown cm-long semiconducting CNT. Using measurement and analysis of Schottky barriers for each metal type across a range of V_g and observation of band-to-band (BTB) tunneling in low-work-function Hf metal, we propose a surface inversion channel (SIC) model that emphasizes carrier transport within the contact-covered section of the CNT. The model provides insight to further understanding of (i) how the contact-related phenomenon can quench electron conduction in low work function metals, (ii) how off-state current often decreases in ambient exposed CNT particularly in the case of large work function metals such as Ti and Pd, and (iii) how gate bias, surface dipole layer, and intrinsic work function affect the path of charge carriers between the metal contact and the CNT channel.

RESULTS AND DISCUSSION

On a single ultra long 1.7 nm diameter semiconducting CNT[17] with an estimated energy gap, $E_g \approx 0.65$ eV,[18] we fabricated FETs with Hf, Ti, Cr, and Pd contacts by e-beam lithography. These metals were chosen because they offer a wide range of work functions (3.9 (Hf)−5.1(Pd)). Devices had 1 μm channel length and were limited to a 40 μm region of the same CNT to further minimize the risk of diameter change. Using temperature-dependent characteristics of thermionic emission, we fit the subthreshold p-type and n-type regions of operation with the basic Schottky model. Richardson plots were constructed and the model was fit for 250 K $< T <$ 300 K to extract zero-bias barrier height estimations.

The activation energy method was used to extract Schottky barrier heights from I_{sd} in terms of gate bias and temperature (see Supporting Information, Figure S1, Figure S2). Hole barriers were extracted as a function of applied gate bias (V_g) for Pd and Ti (Figure 1a), and electron barriers for Hf and Cr FETs (Figure 1b). From these plots we observed that there is (i) a clear exponential relationship between barrier height (Φ_b) and V_g, and (ii) $\partial\Phi_b^{holes}/\partial V_g > \partial\Phi_b^{electrons}/\partial V_g$. Later these relationships will further confirm the validity of the SIC model. Our purpose of the exponential fittings of Figure 1 is to obtain the Schottky barrier height at $V_g = 0$ and determine the E_F of the CNT. Ambiguity occurs in the case of Cr and Hf, where near $V_g = 0$, carrier-type conversion occurs. We assume that for Cr and Hf at $V_g = 0$, the carrier is *n*-type. The barrier height for electron carriers is obtained by extrapolating the linearized log-scale relationships to $V_g = 0$ as shown in Figure 1b (trend lines). The estimated $\Phi_b(V_g = 0)$ can be used to extract a CNT bulk E_F position and subsequent band diagram. All estimations of E_F should be equivalent due to the common CNT and environment of each device. The estimations for E_F are extracted by applying the unpinned level assumption and Schottky Mott relationship ($\Phi_b^{electrons} + \Phi_{metal} = E_F$ and $\Phi_{metal} - \Phi_b^{holes} = E_F$ where Φ_{metal} denotes the metal work function).[19] In the case of Hf, the extrapolated barrier height is far different from the measured barrier height at $V_g = 0$, due to the switch of majority carrier (Table 1). Common work functions are assumed for each metal, including Ti = 4.6,[20] Cr = 4.4,[21] Hf = 4.0, and Pd = 5.0 eV (Supporting Information Table S1). For electron barriers, the extrapo-

TABLE 1. Barrier Heights Extrapolated to $V_g = 0$ Using Least Square Fit for Hole (Pd, Ti) and Electron (Cr, Hf) from *Figure 2*a and Figure 2b, and Measured Values for $V_g = 0$

Φ_b (eV) for $225 < T < 300$ K; $V_{sd} = 0$ V (values in eV)

metal	extrapolated using best fit line	measured
Hf	0.55 (electron)	0.2 (ambiguous)
Cr	0.16 (electron)	0.16 (electron)
Ti	0.11 (hole)	0.11 (hole)
Pd	0−0.1 (hole)	0 0.075(hole)

lated E_F values are 4.55 eV for Hf and 4.56 eV for Cr. For hole barriers, $E_F = 4.5$ eV for Ti and 4.9 eV for Pd.

A few observations can be made from the source−drain current (I_{sd}) and Schottky barrier height as a function of V_g as shown in Figure 2. I_{sd} is inversely proportional to the barrier height. Hole currents are dominant in all the devices regardless of metal contact type and the onset of hole current is $V_g \geq 0$ for all the devices. Hence, E_F of the CNT should be significantly greater than 4.8 eV (electron affinity + $E_g/2$), which is the estimated intrinsic E_F of a 1.7 nm CNT.[18] The observed E_F values above are clearly underestimated and suggest an unusual band alignment near the contacts. We emphasize that this underestimated E_F does not result from inaccurate measurements, since any underestimation of the barrier height violates the Schottky−Mott relationship as $\Phi_b > E_g$ (particularly for the Hf case).[19]

Careful examination of Figure 2 gives insight for different transport phenomena among the metals. For example, Pd has the largest work function, and as expected, has the largest threshold voltage of the metals (Figure 2a). In the case of Ti (Figure 2b), weak ambipolar behavior is observed and more importantly, similar n-type and p-type currents are observed at equal Schottky barrier heights. This suggests that Ti transport has similar properties for both electrons and holes (note that Schottky barrier measurements are offset by gate sweep hysteresis). On the other hand, Hf has the lowest work function and yet has negligible electron current for positive V_g (Figure 2c). The Schottky barriers for Hf closely resemble those of Ti for electron conduction, and are in fact smaller for hole conduction. Measurement yielded nearly constant barriers of 0.1−0.15 eV for $V_g < 0$ V in the case of Hf. It is noted that the hole current is extremely low in spite of low Schottky barrier height and high source−drain bias (V_{sd}). This suggests that Hf has a very thick energy barrier compared to that of Ti, and furthermore, for Hf the electron barrier is thicker than the hole-type barrier. Another intriguing phenomena for Hf near $V_g = 0$ is the existence of a region of negative transconductance, as shown in Figure 2d. This characteristic usually occurs in the case of BTB tunneling[19] and during filling of multiple energy bands during transport.[22] However, multiple energy band conduction is ruled out near $V_g = 0$ V, since E_F is located

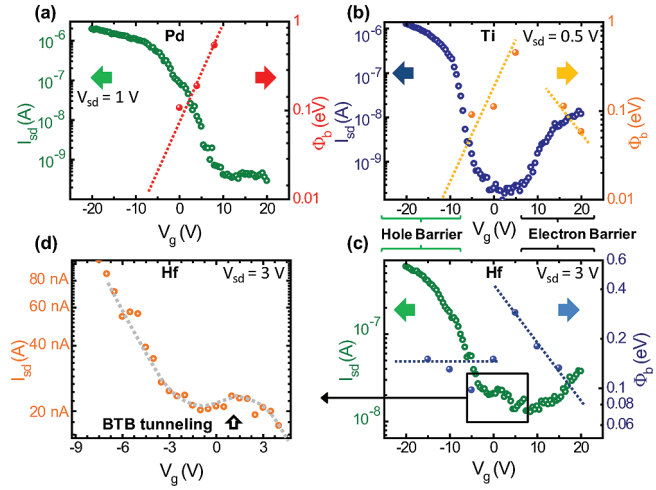

Figure 2. The measured V_g-I_{sd} characteristics and the corresponding barrier height for a given gate bias from (a) Pd p-type device, (b) hole dominant ambipolar Ti device, and (c) hole-dominant ambipolar Hf device. Note that in this case $V_{sd} = 3.0$ V. (d) Negative transconductance at the onset of hole conduction, which is evidence of high source−drain bias BTB tunneling at $V_{sd} = 3.0$.

midgap. The hump was not visible for $V_{sd} \ll 3$ V but appeared in all three Hf devices (same CNT) tested in vacuum with $V_{sd} = 3$ V (Supporting Information, Figure S3). This was only observed in the case of Hf metal, not others.

Using the above Schottky barrier measurements, metal dependent transport characteristics, and the BTB phenomenon, we propose the SIC model and then explain details of the transport phenomena according to this model. The first SIC model presumption is the formation of a CNT inversion layer at the junction. The CNT−metal contact region is strongly affected by gas adsorbates and oxide growth, particularly for low-work function metals, where oxygen exposure can increase surface potential by an eV or more.[20,23] Experimental evidence in the study of oxidation also shows that electric fields enhance native oxide growth. This type of electric field-induced growth produces nonstoichiometric metal oxide species and a reduced activation energy for physisorption or chemisorption at the CNT/metal that can enhance the charge transfer with the CNT.[24] Large field strengths are possible in the local region around the CNT−metal contact to enhance the thickness of oxide or oxygen absorption depth. Therefore, in the case of oxygen exposure, the surface dipole induces electron transfer from the CNT to the metal and typically produces a strongly p-type region that we refer to as the CNT inversion layer. E_F in this region is difficult to modify and will require large gate fields to overcome the screening of the surface dipole. The second presumption is the formation of an additional conduction path through the CNT located under the metal electrode. This CNT region underneath the metal contact is completely resistant to gate fields due to the metal screening, and E_F remains unchanged with ap-

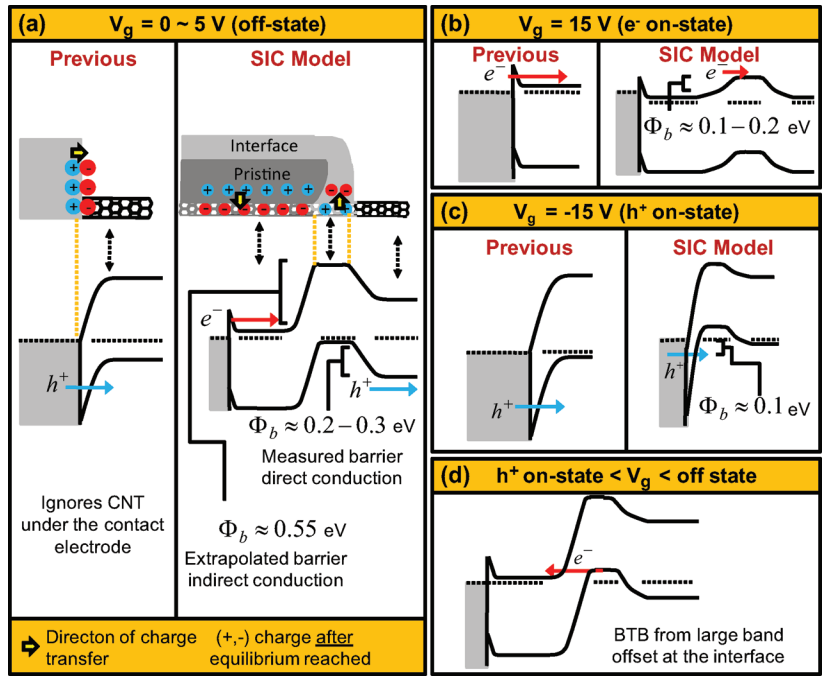

Figure 3. (a) Top panels show the charge transfer between CNT and Hf (low-work-function metal) with exposure to oxygen. The bottom panels show a comparison of a typical band diagram of a surface dipole layer model and our SIC model. In the surface dipole layer model, band bending occurs due to the formation of a dipole layer and the tunnels through the regular Schottky barrier. In the SIC model, three distinct CNT regions are formed: metal-covered CNT, CNT inversion layer, and intrinsic channel. (b) Band diagram of electron conducting on-state at $V_g = 15$ V. An electron barrier between the metal-covered section of the CNT and inversion CNT region dominates conduction. (c) Band diagram of hole conducting on-state at $V_g = -15$ V. Tunneling dominates and transport is governed by direct injection of holes from the metal. (d) The band diagram at a gate bias of intermediate region to show negative transconductance due to BTB tunneling resulting from a large band offset at the interface.

plied V_g. Because of the enhanced growth of a surface oxide layer, which is particularly thick in the case of Hf, the subsurface metal region is protected from adsorbates and will reflect pristine conditions.

Figure 3a shows a schematic of our SIC model for particularly the Hf case (low work function). In the metal-covered CNT region, charge transfer from the metal to the CNT occurs, favoring electron conduction. The direction of the charge transfer of the CNT inversion region is opposite to that of the metal-covered CNT region, favoring hole conduction. This resulting energy band alignment resembles an inversion layer in a metal oxide semiconductor device. To demonstrate the validity of the SIC model, we will explain conduction phenomenon as a function of gate bias. In Figure 3a, the off-state is assumed to occur around $V_g = 0$, although this will depend on gate dielectric and trapped oxide charge. The electron barrier is in agreement with the previously extrapolated value of 0.55 eV. The measured barrier is 0.2 eV with respect to the direct hole conduction, as shown in the schematic.

Electron conduction is favorable at $V_g = 15$ V (Figure 3b), because the metal-covered CNT region has a favorable energy line up for electron conduction with the CNT channel. The "Schottky" barrier observed in the measurements for electron conduction is actually the thick surface inversion layer. The barrier thickness suppresses tunneling current, in agreement with our observations of low electron current in this region. To pass from the electrodes to the CNT, carriers travel first from the metal into the metal-covered CNT, and then traverse the thick inversion layer barrier before entering into the CNT channel. This will be referred to as "indirect transport". Carriers traveling directly from the metal, across the inversion region and into the channel will be referred to as "direct transport". On-state hole transport (at $V_g = -15$ V) is dominated by this direct transport due to severe band bending at the CNT inversion layer interface with the metal (Figure 3c). The subsurface metal contact cannot contribute to the current flow, because E_F is located near the conduction band edge. As a consequence, direct hole transport across the inversion region will be dominated by tunneling and a nearly constant barrier for $V_g < -5$ V, as observed in our measurements.

At the transition region from indirect transport to direct transport ($5\text{ V} < V_g < -5\text{ V}$), a large band offset exists between the subsurface CNT and the CNT inversion layer. With a large enough applied V_{sd}, minority electron carriers from the CNT can tunnel from the valence band of the inversion region to the metal-covered CNT conduction band (Figure 3d). As V_g is decreased (larger negative magnitude) majority hole carriers start to tunnel from the metal and into the inversion layer (direct conduction) as shown in Figure 3C, and the minority electron current decreases. This decrease of mi-

nority carriers gives rise to the brief decrease of the total current, visible as a hump (Figure 2d).

Other metals, including the barrier height measurements of Ti and Pd, are also consistent with the model (Supporting Information Figure S4). Strong hole conduction is observed in Pd due to the p-type nature of both the subsurface and inversion layer (although it is not actually an inversion layer in this context). The off-state occurs when the barrier between the inversion region and CNT channel increases as the gate bias increases. Neither electron conduction nor hole conduction is allowed owing to the lack of an indirect or direct transport path for large positive V_g. Therefore, no ambipolar behavior can be expected in the case of Pd metal. For Ti, on the other hand, increased ambipolar conduction is observed when compared with metal contacts having much lower work function due to favorable direct conduction of both hole and electron carriers. The work function of Ti (4.6 eV) is located 0.1−0.2 eV below the conduction band minimum of CNT (in the band gap) and limits indirect hole conduction in the presence of a surface dipole. However, the CNT inversion layer E_F is located closer to the valence band, permitting larger directly injected current. The Schottky barrier for direct conduction of electron current in the case of Ti is smaller than in the case of Hf and Pd. This direct mechanism is in addition to a small indirect flow of electrons, allowing weak ambipolar behavior even in the presence of a surface dipole (Supporting Information Figure S4). The direct transport mechanism dominance is further confirmed due to the equivalent hole and electron currents at equal measured Schottky barrier heights (Figure 2b).

After considering each metal independently, we also note that the differences in $\partial\Phi_b^{holes}/\partial V_g$ and $\partial\Phi_b^{electrons}/\partial V_g$ from Figure 1 must be a direct consequence of $|\partial E_F^{inversion}/\partial V_g| \ll |\partial E_F^{channel}/\partial V_g|$. The value of $\partial E_F^{inversion}/\partial V_g \propto \partial\Phi_b^{electrons}/\partial V_g$ is strongly limited by the dipole induced screening. Meanwhile, $\partial E_F^{channel}/\partial V_g \propto \partial\Phi_b^{holes}/\partial V_g$ is unaffected by dipoles and related only to the gate/CNT coupling. A significantly large value of $\partial\Phi_b^{holes}/\partial V_g$ is observed in our measurements, as evidenced by the electrical measurements in Figure 2 for Ti and Pd. Additionally, we suggest that the previously observed decreases in on-state hole current[14] after annealing or high vacuum degassing are the consequence of a weakened CNT inversion region and not a significant variation in work function. The inversion region remains p-type, but E_F shifts closer to midband gap as oxygen desorbs. The result is a thicker barrier for hole conduction and a decrease in tunneling current. The appearance of a weak electron conducting on-state can occur if desorption weakens the dipole significantly, similar to recent reports.[14]

CONCLUSION

In conclusion, a surface inversion channel model, which includes two competing pathways for carrier transport, has been proposed to explain the anomalous barrier heights and a transconductance hump in our experimental results. This model clearly explains why ohmic contacted n-type devices are difficult to achieve. For air-stable electron conduction, a low-work-function metal with weak surface dipole must be utilized for CNT contact. The inversion channel model is in agreement with previous results by other groups and should serve as a basic outline for adsorbate exposed CNT-FET conduction.

METHODS

Carbon Nanotube Growth. Ultralong aligned CNTs were synthesized by laminar flow thermal chemical vapor deposition (First Nano, Easy Tube) with $FeCl_3$ (Sigma Aldrich) in ethanol as a catalyst using a method similar to that described in ref 17. Optimal growth flow rates were 16 sccm H_2, 8 sccm CH_4, and 100 sccm Ar with laminar flow enhancement using a smaller $^1/_2$ in. quartz tube placed within the larger 2 in. tube. These conditions were ideal for centimeter or longer (substrate limited) aligned CNT growth, with sparse CNT spacing ~100 μm.

CNT-FET Fabrication. After CNT growth, e-beam lithography (EBL, Raith E-Line) patterning was used to define alignment markers that were subsequently etched into the SiO_2 with 9:1 buffered oxide etch (Hf). Using a scanning electron microscope, we first examined the area near the catalyst region to locate a desirable CNT. As the CNTs are strongly aligned, 1 mm steps were taken along the same CNT to denote its exact location without exposing the future device regions to the electron beam. To contact the CNT with metal electrodes, hundreds of large probeable pads (modular design) were fabricated with lead lines approaching within ~15 μm of the CNT. Individual metal contact species were then patterned with EBL, metal was deposited by e-beam evaporation, and lift-off was performed in 45 °C acetone. Post fabrication, CNT-FETs regions were covered with optical photoresist, and the sample was etched in 100−150 W O_2 plasma to remove other CNTs.

Electrical Measurements. Measurements were performed in a closed cycle refrigerator over the temperature range 150−300 K. Electrical measurements were collected with a Keithley 236 (source/drain) and Keithley 237 (gate/drain) with automated Labview interface.

Acknowledgment. The Pittsburgh group would like to acknowledge the Air Force Office of Scientific Research through a grant provided by MOEST and NSF OISE No. 0820918. The SKKU group would like to thank KICOS through a grant provided by MOEST in 2007 (No. 2007-00202), by the STAR-faculty project, TND Project, WCU program through the NRF funded by the MOEST (R31-2008-000-10029-0), and the NRF through CNNC at SKKU.

Supporting Information Available: Details regarding measurement of barrier heights; electrical measurements as a function of temperature for various metals in the hole subthreshold regime (Figure S1); barrier heights for Hf, Cr, Ti, and Pd by applied V_g and V_{sd} using the thermionic model (Figure S2); observation of high bias negative transconductance in three other Hf devices on the same CNT (Figure S3); work function data for each metal explained using previous literature results (Table S1); energy

band diagrams for Cr, Ti, and Pd devices at various applied V_g (Figure S4). This material is available free of charge *via* the Internet at http://pubs.acs.org.

REFERENCES AND NOTES

1. Zhu, W.; Bower, C.; Zhou, O.; Kochanski, G.; Jin, S. Large Current Density from Carbon Nanotube Field Emitters. *App. Phys. Lett.* **1999**, *75*, 873–875.
2. Javey, A.; Guo, J.; Farmer, D. B.; Wang, Q.; Wang, D.; Gordon, R. G.; Lundstrom, M.; Dai, H. Carbon Nanotube Field-Effect Transistors with Integrated Ohmic Contacts and High-k Gate Dielectrics. *Nano Lett.* **2004**, *4*, 447–450.
3. Yu, W. J.; Kim, U. J.; Kang, B. R.; Lee, I. H.; Lee, E. H.; Lee, Y. H. Adaptive Logic Circuits with Doping-Free Ambipolar Carbon Nanotube Transistors. *Nano Lett.* **2009**, *9*, 1401–1405.
4. Zhang, Z.; Liang, X.; Wang, S.; Yao, K.; Hu, Y.; Zhu, Y.; Chen, Q.; Zhou, W.; Li, Y.; Yao, Y.; *et al*. Doping-Free Fabrication of Carbon Nanotube Based Ballistic CMOS Devices and Circuits. *Nano Lett.* **2007**, *7*, 3603–3607.
5. Yu, W. J.; Jeong, S. Y.; Kim, K. K.; Kang, B. R.; Bae, D. J.; Lee, M.; Hong, S.; Prabhu Gaunkar, S.; Pribat, D.; Perello, D.; *et al*. Bias-Induced Doping Engineering with Ionic Adsorbates on Single-Walled Carbon Nanotube Thin Film Transistors. *New J. Phys.* **2008**, *10*, 113013.
6. Lin, Y. M.; Appenzeller, J.; Avouris, P. Ambipolar-to-Unipolar Conversion of Carbon Nanotube Transistors by Gate Structure Engineering. *Nano Lett.* **2004**, *4*, 947–950.
7. Charlier, J. C.; Blase, X.; Roche, S. Electronic and Transport Properties of Nanotubes. *Rev. Mod. Phys.* **2007**, *79*, 677–732.
8. Freitag, M.; Tsang, J. C.; Bol, A.; Yuan, D.; Liu, J.; Avouris, P. Imaging of the Schottky Barriers and Charge Depletion in Carbon Nanotube Transistors. *Nano Lett.* **2007**, *7*, 2037–2042.
9. Xue, Y.; Ratner, M. A. Scaling Analysis of Schottky Barriers at Metal-Embedded Semiconducting Carbon Nanotube Interfaces. *Phys. Rev. B* **2004**, *69*, 161402.
10. Chen, Y. F.; Fuhrer, M. S. Tuning from Thermionic Emission to Ohmic Tunnel Contacts *via* Doping in Schottky-Barrier Nanotube Transistors. *Nano Lett.* **2006**, *6*, 2158–2162.
11. Shim, M.; Javey, A.; Kam, N. W. S.; Dai, H. Polymer Functionalization for Air-Stable n-Type Carbon Nanotube Field-Effect Transistors. *J. Am. Chem. Soc.* **2001**, *123*, 11512–11513.
12. Heinze, S.; Tersoff, J.; Martel, R.; Derycke, V.; Appenzeller, J.; Avouris, P. Carbon Nanotubes as Schottky Barrier Transistors. *Phys. Rev. Lett.* **2002**, *89*, 106801.
13. Xiaodong, C.; Freitag, M.; Martel, R.; Brus, L.; Avouris, P. Controlling Energy-Level Alignments at Carbon Nanotube/Au Contacts. *Nano Lett.* **2003**, *3*, 783–787.
14. McClain, D.; Thomas, N.; Youkey, S.; Schaller, R.; Jiao, J.; O'Brien, K. P. Impact of Oxygen Adsorption on a Population of Mass Produced Carbon Nanotube Field Effect Transistors. *Carbon* **2009**, *47*, 1493–1500.
15. Collins, P. G.; Arnold, M. S.; Avouris, P. Engineering Carbon Nanotubes and Nanotube Circuits Using Electrical Breakdown. *Science* **2001**, *292*, 706–709.
16. Nosho, Y.; Ohno, Y.; Kishimoto, S.; Mizutani, T. Relation Between Conduction Property and Work Function of Contact Metal in Carbon Nanotube Field-Effect Transistors. *Nanotechnology* **2006**, *17*, 3412–3415.
17. Ding, L.; Tselev, A.; Wang, J.; Yuan, D.; Chu, H.; McNicholas, T. P.; Li, Y.; Liu, J. Selective Growth of Well-Aligned Semiconducting Single-Walled Carbon Nanotubes. *Nano Lett.* **2009**, *9*, 800–805.
18. Weisman, R. B.; Bachilo, S. M. Dependence of Optical Transition Energies on Structure for Single-Walled Carbon Nanotubes in Aqueous Suspension: An Empirical Kataura Plot. *Nano Lett.* **2003**, *3*, 1235–1238.
19. Sze, S. M. *Physics of Semiconductor Devices*; Wiley-Interscience: New York, 1981.
20. Jonker, B. T.; Morar, J. F.; Park, R. L. Surface States and Oxygen Chemisorption on Ti(0001). *Phys. Rev. B* **1981**, *24*, 2951–2957.
21. Szadkowski, A. J.; Kalnitsky, A.; Ma, K. B.; Zukotynski, S. Implications of the Change in Work Function of Chromium by the Presence of Hydrogen on the Properties of Electrical Contact Between Chromium and Hydrogenated Amorphous Silicon. *J. Appl. Phys.* **1982**, *53*, 557–558.
22. Appenzeller, J.; Knoch, J.; Radosavljevic, M.; Avouris, P. Multimode Transport in Schottky-Barrier Carbon-Nanotube Field-Effect Transistors. *Phys. Rev. Lett.* **2004**, *92*, 226802.
23. Ustaze, S.; Lacombe, S.; Guillemot, L.; Esaulov, V. A.; Canepa, M. Electron Transfer on Oxygen-Covered Ag(110) and Al(111) Surfaces: Work Function *versus* Local Electronic Effects. *Surf. Sci.* **1998**, *414*, 938–944.
24. Sankaranarayanan, S. K. R. S.; Kaxiras, E.; Ramanathan, S. Electric Field Tuning of Oxygen Stoichiometry at Oxide Surfaces: Molecular Dynamics Simulations Studies of Zirconia. *Energy Environ. Sci.* **2009**, *2*, 1196–1204.